Exploring cyclic aminopolycarboxylate ligands for Sb(III) complexation: PCTA and its derivatives as promising solution

Enikő Tóth-Molnár,[§] Norbert Lihi,[†] Gyula Tamás Gál,[§] Sourav De,[‡] Petra Bombicz,[‡] István Bányai,[§] Dezső Szikra,[⁑] Eleonóra Dénes,[ǂ] Gyula Tircsó[§], Imre Tóth[§†] and Ferenc Krisztián Kálmán,[§]*

[§]Department of Physical Chemistry, Faculty of Science and Technology, University of Debrecen, H-4032 Debrecen, Hungary

[†]Department of Inorganic and Analytical Chemistry, Faculty of Science and Technology, University of Debrecen, H-4032 Debrecen, Hungary

[‡]Research Laboratory of Chemical Crystallography, Research Centre for Natural Sciences, H-1117 Budapest, Hungary

[⁑]Division of Nuclear Medicine and Translational Imaging, Department of Medical Imaging, University of Debrecen, H-4032 Debrecen, Hungary

[ǂ]Centre of Supramolecular Organic and Organometallic Chemistry, Department of Chemistry, Babeş-Bolyai University, RO-400028 Cluj-Napoca, Romania

ABSTRACT: In the recent years the Auger electron emitters have been suggested as promising candidates for side effect free radiotherapy in cancer treatment. In this work we report a detailed coordination chemistry study on [Sb(PCTA)] (PCTA: 3,6,9,15-tetraazabicyclo[9.3.1]pentadeca-1(15),11,13-triene-3,6,9-triacetic acid), a macrocyclic aminopolycarboxylate type complex of antimony(III), whose ^{119}Sb isotope could be a suitable low-energy electron emitter for radiotherapy. The thermodynamic stability of the chelate obtained by pH-potentiometry and UV-vis spectrophotometry is high enough ($\log K_{[Sb(PCTA)]}$ = 23.2(1)) to prevent the hydrolysis of metal ion near physiological pH. The formation of [Sb(PCTA)] is confirmed by NMR and ESI-MS measurements in solution, furthermore the structure of [Sb(PCTA)]·NaCl·3H_2O and [Sb(PCTA)]·HCl·3H_2O is described by X-ray diffraction and DFT calculations. Consequently, the [Sb(PCTA)] is the first thermodynamically stable antimony(III) complex bearing polyamino-polycarboxylate macrocyclic platform. Our results demonstrate the potential of rigid (pyclen derivative) ligands as chelators for future application of Sb(III) in the targeted radiotherapy based on ^{119}Sb isotope.

Introduction

Cancer, a terrifying word covers the most diverse disease, which was responsible for 9.6 million deaths worldwide in 2018 according to the report of WHO.[1] Despite the huge research efforts devoted to find a cure for its more than 120 types in the last decades, the available therapy options are often limited, possessing unwanted side effects. The situation is similar with radiotherapy, one of the most powerful weapons against cancer, in which the radiation directly kills cancer cells.

Although significant improvement in focusing the radiation more precisely to the tumor recently resulted from new technologies in radiation therapy, some of the healthy tissues are always affected. Obviously, the implementation of a side effect free modality within radiotherapy is a long-desired goal and would be a significant progress in cancer treatment.

The use of Auger electron emitters such as ^{111}In, ^{67}Ga, ^{99m}Tc, ^{123}I, ^{201}Tl etc., offers a solution to this problem, especially in the treatment of micrometastases and small tumors due to their highly localised energy deposition based on their nano- to micrometer range and high linear energy transfer (LET).[2–4]

One of the most promising radioisotopes among the low-energy electron emitters is the ^{119}Sb thanks to its excellent decay properties. The ^{119}Sb decays with electron capture (100% branching) with a half-life ($t_{1/2}$) of 38.19 h. Beside the low energy gamma peak at 3.87 keV (16.1%) it emits 23.7 Auger electrons per decay, with an average energy of 0.4 keV (in the 0.5-1 nm range) as well as 0.8 internal conversion electrons with an average energy of 20.2 keV.[2] The lack of the high energy γ rays in the decay ensures the short range effect and enables the use of high radiation doses (even GBq) with fewer side effects.[2] Decreasing the side effects of targeted isotope therapy becomes more and more important, as this treatment option gradually shifts from rarely used salvage therapy to a standard protocol available for a larger number of patients. Why are the ^{119}Sb isotopes not widely used yet? The answer is the limited access to the radiometal due to the difficulties in production and purification, which seem to be solved recently by Bennett and co-workers at Los Alamos National Laboratory.[5] The new method offers an alternative, long-time period access to the ^{119}Sb by using ^{119m}Te isotope (half-life, $t_{1/2}$ = 4.7 days) as mother element[6] instead of the direct production with cyclotron which is rarely available in clinical practice.[7]

The internalization and/or DNA binding of the radionuclides obligate their complexation with a suitable bifunctional ligand for targeting purposes possessing high thermodynamic stability as well as inertness to avoid the *in vivo* decomplexation. In case of suitable ligand(s) of Sb(III) for targeted theragnostics the ^{119}Sb would be one of our most important weapon in the war against cancer.

Wide range of Sb(III)/(V) complexes were studied involving mostly S donor ligands,[8] but only two aminopolycarboxylate complexes showing antitumor activity have been found so far. The NH_4^+ and Na^+ salts of $[Sb(NTA)(HNTA)]^{2-}$ were found to be effective against Ehrlich adenocarcinoma tumor,[9] while NH_4(Sb[HPDTA]) showed cytotoxicity in human promyelocytic leukemia (HL-60) cells.[10,11]

The Sb(III) with its 0.76 Å ionic radius and 3+ charge is generally recognized as a borderline Lewis acid (less frequently as hard acid) possessing high affinity towards nitrogen-, oxygen- and thiolate-containing ligands.[12–14] In its coordinative compounds the CN mostly is 4, 5 or 6 and the structure of the complexes is often a non-symmetrical coordination polyhedron due to the presence of the stereochemically active lone pair (s^2) electrons.[15] The limited ability of aminopolycarboxylate chelators for Sb(III) complexation can be attributed to the strong tendency of the Sb(III) to hydrolyze in aqueous solution provoking the loss of the metal from its complexes, i.e. the formation of the solid Sb_2O_3 in near-neutral and basic conditions. Özer and Bogucki[16] stated that the Sb(III) complexes formed with H_4EDTA, H_3HEDTA and H_5DTPA ligands (the structure of the ligands together with others mentioned in the text are presented in the ESI, Scheme S1) were stable in acidic conditions forming [Sb(L)] and [Sb(HL)] species; and the hydrolysis of the metal ion was observed above pH=6. Preparation of several Cat^+[Sb(EDTA)] in aqueous solution at pH = 5 - 7 has been published by Ilyukhin and Davidovits.[17] To the best of our knowledge, no polyamino-polycarboxylate macrocyclic complexes of Sb(III) have been published so far.

In this study, we present the coordination chemical characterization of the new [Sb(PCTA)] complex. H_3PCTA (Scheme 1.) has been selected from a group of amino-carboxylates consisting of both open-chain and macrocyclic ligands. Furthermore, the H_3PCTA ligand and its derivatives have been recently successfully used for the complexation of paramagnetic metal ions (e.g. Mn (II), Gd (III), etc.) which made us include the given ligand in the screeening.[18,19] The thermodynamic stability and inertness of the complex have been investigated by means of pH-potentiometric and UV-vis spectrophotometric methods while the structure of the complex has been determined by single crystal X-ray diffraction and DFT calculations. Furthermore, to prove the exclusive existence of the [Sb(PCTA)] chelate in near-neutral conditions, MS and NMR measurements have also been carried out.

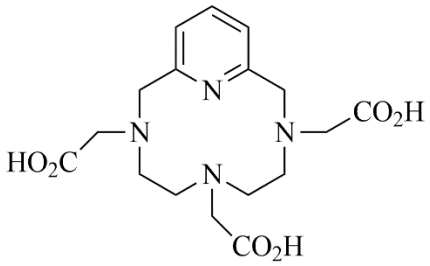

Scheme 1. The structure of H_3PCTA.

Results and discussion

In order to find the best platform for the chelation of Sb(III), preliminary experiments were carried out with several open-chain and macrocyclic ligands (H_3NOTA, H_4DOTA, H_3DO3A, H_2tDO2A, H_2tO2DO2A, H_3PCTA, H_2BP2A, H_4AAZTA, H_5DTPA, H_4CDTA, H_2CDTA-nSer, Scheme S1). The Sb(III) (in HCl solution) and the given ligand was mixed in 1 to 1 metal to ligand ratio at 2.5 mM concentration forming homogenous solutions. The appearance of the

$Sb(OH)_3/Sb_2O_3$ could easily be observed visually. The pH adjustment was done by adding droplets of concentrated NaOH solution at high stirring rate until reaching neutral pH. The cloudy solutions (suspensions) then were stirred and kept at high temperature (70 °C) for 5-7 days. (Samples possessing white precipitation, presumed to be Sb_2O_3, based on literature evidences[16], were not analyzed further.) The pH was checked in the cooled samples at room temperature. None of the samples except Sb(III)-H_3PCTA were homogenous. The reaction mixture was measured by ESI-MS and the presence of the desired [Sb(PCTA)] was detected ($[C_{17}H_{21}N_4O_6Sb+Na]^+$, found: 521.0398; calculated: 521.0391, Figure S1). The ESI-MS experiments were carried out also in negative mode but unfortunately, they did not deliver reasonable results, since the peaks of the ternary–hydroxido complexes did not appear.

Further detailed experiments with H_4DOTA and different Sb-precursors (Sb_2O_3, Sb_2(tartrate)$_2$, $SbCl_3$) were carried out in different conditions, but none of them resulted in quantitative formation of $[Sb(DOTA)]^-$. H[Sb(EDTA)] and Na[Sb(EDTA)] solids were prepared following the recipes described in literature.[17] ^{1}H NMR spectra of these complexes showed one set of signals, an AB-multiplet of the acetate protons and a singlet of the ethyl protons in distilled water, indicating the solution stability of the complexes at pH<7. Transchelation reaction of $[Sb(EDTA)]^-$ with H_2DOTA^{2-} (1:1 molar ratio) followed by ^{1}H NMR was slow and far from complete after 15 days (Figure S2). These experimental findings call for further study to find suitable ligands and/or preparation “tricks” to get stable, water soluble Sb(III)-complexes.

On the basis of preliminary results, we selected the macrocyclic H_3PCTA for detailed characterization.

Beside the mass spectrometric measurement 1D (^{1}H) and 2D (COSY and DOSY) experiments were carried out on samples containing $PCTA^{3-}$ ligand and Sb(III) – PCTA system in

1 to 1 metal to ligand ratio dissolved in D_2O at neutral pH to confirm the complex formation. The assignment of the ^{1}H-NMR signals was carried out based on the results of 2D COSY (Figure S3) in agreement with the published data by Aime et al. (see ESI).[19]

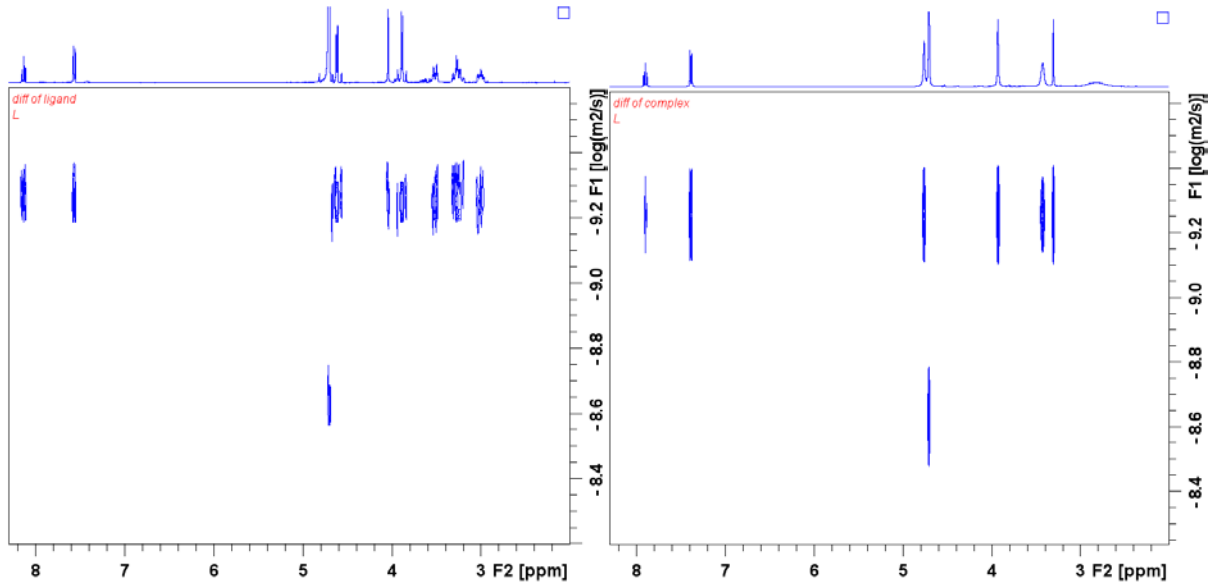

Figure 1. 2D DOSY spectra of free ligand (left) and the Sb(III) complex (right).

The disappearance of the fine structure of the ^{1}H spectrum in the presence of Sb(III) is the result of the intramolecular motion (i.e. the alternation of acetate pendant arm) of the complex (Figure S4). This significant change in the ^{1}H spectrum could be explained by a strong interaction between the Sb(III) and $PCTA^{3-}$ thanks to the complex formation. However, the strong interaction does not mean that the formed complex is rigid in structure. Even the complexes of certain macrocyclic ligands are known to display some fluxionality in solution.[19] The disappearance of the fine structure of the spectra and the line broadening of the peaks is likely to cause the lack of COSY cross-peaks (Figure S4 and S5). Nevertheless, the comparison of the signal intensities of the $PCTA^{3-}$ in the presence and absence of Sb(III) also suggests the existence of ML complex in

solution (Figure S6). 2D DOSY (diffusion ordered spectroscopy) spectra were also recorded to prove the formation of the monomer complex [Sb(PCTA)] without the appearance of dimers or oligomers. The DOSY spectra of the ligand (Figure 1.) showed two lines, one for the water and one for the PCTA since the water molecule has faster dynamics in solution. The same situation was observed for the Sb(III)-$PCTA^{3-}$ system, which means that only one PCTA containing species is present in solution. The DOSY technique is also able to deliver information on the diffusion coefficient of the different species presented in solution. There was no significant difference between the diffusion coefficient of the complex and the free ligand (Figure S7 and S8). In other words, the hydrodynamic size did not change much upon the complex formation. It was also observed that only two dominant cross peaks appeared, the faster one was the water the slower one was either the complex or the ligand. The diffusion coefficients could be calculated from the 1D evaluation of the DOSY and were $(4.7 \pm 0.1) \times 10^{-10}$ m^2 s^{-1} and $(4.6 \pm 0.1) \times 10^{-10}$ m^2 s^{-1}, respectively.

The thermodynamic features of the [Sb(PCTA)] complex were studied by pH-potentiometric and UV-vis spectrophotometric methods in the presence of NaCl as ionic strength (I=0.15 M) at 25 °C. The protonation constants of the ligand and the (preformed) Sb(III) complex were determined by direct pH-potentiometric titrations, whereas the stability of the chelate was investigated by spectrophotometry using an out-of-cell (batch) method at high acid concentration since the complex formation is already complete at pH = 1, and the equilibration time could be substantial at high acid content. Then the data collected by pH-potentiometric and UV-vis spectrophotometric methods were fitted separately to evaluate the equilibrium constants (see ESI).

Since the formation of the Sb(III) complexes occurs in the 0.1 – 1.0 M proton concentration range, the protonation constants of the H_3PCTA ligand have been determined for 1.0 M NaCl/HCl

ionic strength. Four protonation constants have been obtained as follows: 9.08(1), 7.31(2), 3.80(2) and 2.43(1). According to the studies performed by Aime et al.[19] on the protonation sequence of H_3PCTA, the first two constants feature the protonation process of the macrocyclic N donor atoms, while the third and fourth protonation occurs on the acetate pendants.

Two extra base-consuming steps appeared in addition to the four dissociating H^+ of the ligand for the [Sb(PCTA)] in the pH-range 6.8 - 8.6 (Figure S9, 0.15 M and 25 °C) related to the formation of two ternary hydroxido complexes ($[Sb(OH)(PCTA)]^-$ and $[Sb(OH)_2(PCTA)]^{2-}$) followed by the breakdown of the complex and hydrolysis of the Sb(III) above pH 9. To make sure that the ternary hydroxo complexes are real equilibrium species, not only the artifacts of the slow hydroxo-assisted dechelation of the complex, batch samples containing 2.5 mM [Sb(PCTA)] in the pH range 7 to 8 were prepared, and were found stable, precipitation was not visible after several weeks. Furthermore, the ligand exchange reactions were also carried out (see below) in the given pH range which also support our equilibrium model.

Because of the high stability of the [Sb(PCTA)] 9 batch samples, containing the Sb(III) and the ligand in 0.2 mM concentration and increasing concentration of HCl, were prepared. The samples were set aside for one day to reach the equilibrium and the absorption spectra were recorded between 200-400 nm (Figure S10). In order to avoid the interference originating from the different ionic strength concentrations the spectrophotometric and pH-potentiometric data were fitted separately by using the designated computational program PSEQUAD.[20] During the fitting procedure, the standard deviation of the values and the fitting parameter decreased significantly when the formation of a protonated species ($[Sb(HPCTA)]^+$) was also considered. For this reason, the equilibrium data were fitted by assuming the existence of $[Sb(HPCTA)]^+$ when fitting the UV-vis data, while $[Sb(HPCTA)]^+$, [Sb(PCTA)], $[Sb(OH)(PCTA)]^-$ and $[Sb(OH)_2(PCTA)]^{2-}$ species

were applied for the pH-potentiometric titration data, respectively (see ESI for further details). The stability and protonation constants were defined by Equations 1-4 (the square brackets in the equations show equilibrium concentrations of species).

$$K_{\mathrm{Sb(PCTA)}} = \frac{[\mathrm{Sb(PCTA)}]}{[\mathrm{Sb(III)}][\mathrm{PCTA}^{3-}]} \quad (1)$$

$$K^{\mathrm{H}}_{\mathrm{Sb(PCTA)}} = \frac{[\mathrm{Sb(HPCTA)}^{+}]}{[\mathrm{Sb(PCTA)}][\mathrm{H}^{+}]} \quad (2)$$

$$K^{\mathrm{OH}}_{\mathrm{Sb(PCTA)}} = \frac{[\mathrm{Sb(PCTA)(OH)}^{-}][\mathrm{H}^{+}]}{[\mathrm{Sb(PCTA)}]} \quad (3)$$

$$K^{\mathrm{OH}}_{\mathrm{Sb(PCTA)(OH)}} = \frac{[\mathrm{Sb(PCTA)(OH)}_2^{2-}][\mathrm{H}^{+}]}{[\mathrm{Sb(PCTA)(OH)}^{-}]} \quad (4)$$

The equilibrium constants of the different species were log$K_{[\mathrm{Sb(PCTA)}]}$ = 23.2(1), log$K^{\mathrm{H}}_{[\mathrm{Sb(PCTA)}]}$ = 2.40 (1), log$K^{\mathrm{OH}}_{[\mathrm{Sb(PCTA)}]}$ = -7.30(6) and log$K^{\mathrm{OH}}_{[\mathrm{Sb(PCTA)(OH)}]-}$ = -7.63(3), respectively. The stability constant of the Sb(III) complex was also calculated by taking into account the formation constants of the Sb(III)-chlorido and hydroxido complexes gained from different sources (Figure S11A-D)[21–25] delivering values in the range of 25.2–31.5. A similar value (log$K_{[\mathrm{Sb(CDTA)}]-}$ = 24.8) was reported by Wang Er-kang[26] for the $[\mathrm{Sb(CDTA)}]^{-}$ complex using 4.0 M NaCl as an ionic strength, however, the formation of the chlorido complexes was not taken into account by the authors.[14] The stability of the $[\mathrm{Sb(EDTA)}]^{-}$ was found to be 19.5 log units in the same work under similar conditions. The species distribution diagram for the system of Sb(III) –

PCTA – Cl^- – H^+ is showed in Figure 2., which confirms the existence of ternary hydroxydo complexes near physiological pH.

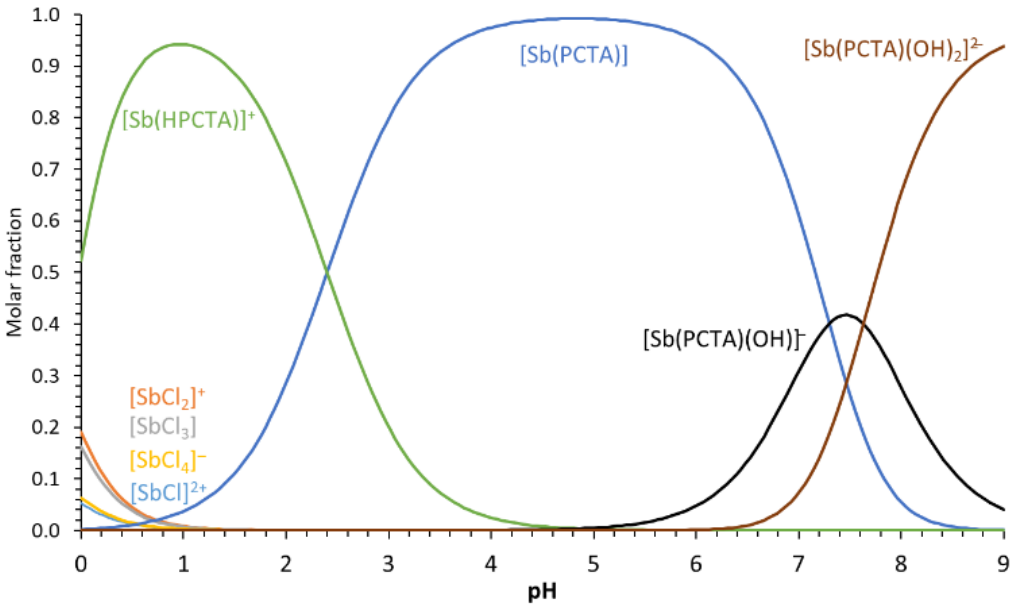

Figure 2. Species distribution diagram of the Sb(III) – PCTA – Cl^- – H^+ system ([Sb(III)] = [$PCTA^{3-}$] = 2.0 mM and [Cl^-] = 1.0 M).[21]

Going back to the matter of the ternary complexes (see above), the separated samples were stable for weeks in the pH range between 7 – 8 and the dechelation of the [Sb(PCTA)] followed by the formation of antimony-trioxide was not observed. Furthermore, the presence of the chelate was also established by high-resolution mass spectrometric (ESI) analysis of the same sample at pH 7.0 (Figure S1), surprisingly only confirming the Na^+-adduct of the [Sb(PCTA)]. Actually, the gas phase can hardly imitate the alkaline solutions. (NMR spectra recorded for the sample of [Sb(PCTA)] complex in D_2O at neutral pH (pD=7.25) after 2 days and 3 months were identical which also support the formation of hydroxido species in equilibrium (Figure S4 and S5).

Taking a closer look to the inertness of the complex, ligand exchange reactions were performed in the pH range 5.5 to 7.0 in the presence of 10, 20 and 40-fold excess of tartrate as a scavenger for the Sb(III) ion. The progress of the exchange reactions was monitored by spectrophotometry on the absorption band of $PCTA^{3-}$. Since the high excess of the tartrate ensures the pseudo-first order condition for the exchange reactions, the k_{obs} calculated for each reaction is a pseudo-first order rate constant (Equation 5).

$$-\frac{\mathrm{d[Sb(PCTA)]_t}}{\mathrm{d}t} = k_{\mathrm{obs}}[\mathrm{Sb(PCTA)}]_\mathrm{t} \quad (5)$$

where $[Sb(PCTA)]_t$ is the total concentration of the complex.

Furthermore, the fitting of the k_{obs} values gained at different exchanging ligand concentrations can deliver information on the role of the tartrate in the dissociation reactions.

Knowing the high affinity of Sb(III) towards hydrolysis it was not surprising that the k_{obs} values increase with decreasing acid concentration (i.e. increasing pH, Figure 3). However, the impact of the tartrate ion on the reaction rate was unexpected since the k_{obs} values decrease with increasing tartrate concentration (Figure 3). A similar phenomenon was described for the metal exchange reactions of some polyamino-polycarboxylate complexes when the formation of a stable dinuclear intermediate ([M(L)M']), the so-called "dead-end" complex, slows down the reactions by competing with other reaction pathways.[27] In our view the formation of a stable ternary tartrate complex can effectively reduce the concentration of the $[Sb(OH)(PCTA)]^-$, an intermediate responsible for the OH^--assisted dissociation pathway. Plotting of k_{obs} against $[OH^-]$ resulted in straight lines with significant intercepts (Figure 3), thus the exchange reaction occurs *via* spontaneous (k_0) and hydroxide-assisted pathways (k_1).

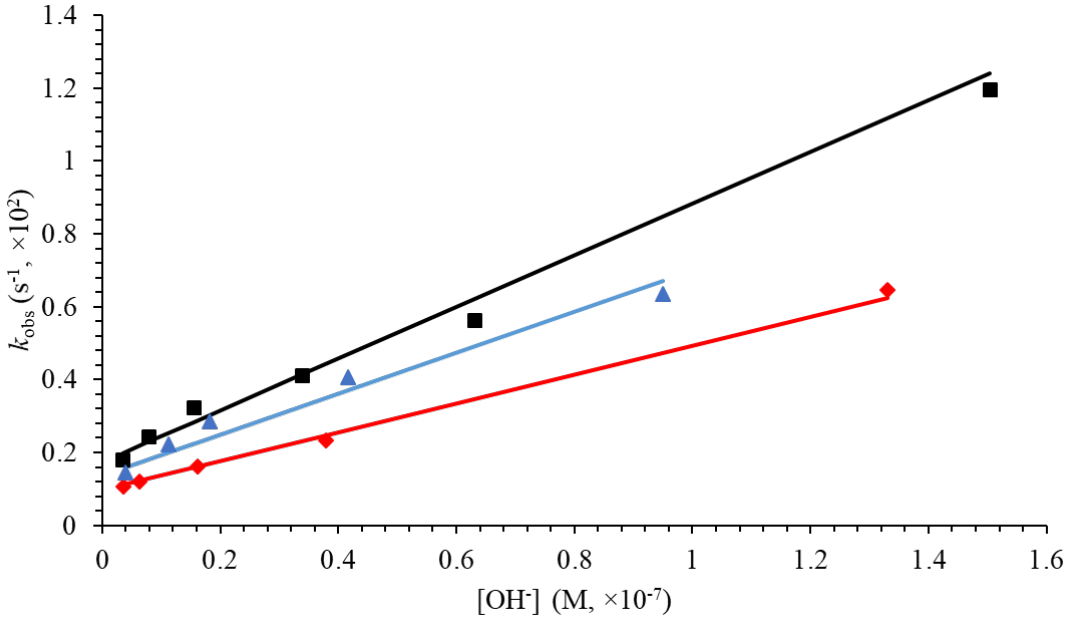

Figure 3. Dependence of the pseudo-first-order rate constants (k_{obs}) on the [OH^-] for the [Sb(PCTA)] complex at 10- (■), 20- (▲) and 40-fold (♦) excess of tartrate. The lines correspond to the best fit of the k_{obs} values.

Taking into account all the observations the rate law can be expressed as follows:

$$k_{obs} = \frac{k_0 + k_1[OH^-]}{1 + K_L[L]} \quad (6)$$

where $k_1 = k_{OH} * K_{SbPCTA}^{OH}$, k_{OH} is the rate constant characterizing the dissociation of the [Sb(PCTA)(OH)]$^-$ species and K_L is the stability constant of the ternary [Sb(PCTA)(tartrate)] complex (K_L=[Sb(PCTA)(tartrate)]/[Sb(PCTA)][tartrate]). Figure 3 shows the best fit of the k_{obs} values. The values obtained for k_0, k_1 and K_L are (2.4±0.2)×10^{-3} s^{-1}, (9.7±0.8)×10^4 $M^{-1}s^{-1}$ and

180±30 M^{-1} ($\log K_L$=2.3±0.1), respectively. Using the rate constants characterizing the spontaneous and hydroxide-assisted dissociation pathways, the half-life ($t_{1/2}$) of the complex at different pH values can be calculated. The $t_{1/2}$ values ($t_{1/2}=\ln 2/k_{obs}$) were found to be 82.0, 7.0 and 1.8 s for pH 6.8, 8.0 and 8.6, respectively. These results confirm the assumption that the ternary-hydroxo complexes cannot be artificial species, since above pH 8 the hydrolysis of the complex would become significant (the time of the total reaction is approximately 7 $t_{1/2}$). (The waiting time after addition of each dose of titrant NaOH was long enough in the alkaline region, about 40 s during the titration.) Unfortunately these $t_{1/2}$ values also clearly show that the inertness of the [Sb(PCTA)] is quite low near physiological pH, which is not favourable for the *in vivo* applications. In order to gain information on the structure of the complex and its kinetic lability further theoretical and X-Ray studies were carried out.

The crystals grown from methanolic solutions of the complex (PCTA-Sb1 (NaCl) and PCTA-Sb2 (HCl)) were suitable for single crystal X-ray diffraction. The complexes crystallized in the monoclinic crystal system in $P2_1/n$ space group with the inclusion of three water molecules per asymmetric unit. In case of PCTA-Sb1, the crystal contains an additional Na^+ ion per asymmetric unit compared to the PCTA-Sb2 crystal structure, originating from the neutralisation of the solution. The ORTEP representation of the compounds are shown in Figure 4. In both crystals, the Sb(III) ion is accommodated by the $PCTA^{3-}$ ligand with its N1, N2, N3, N4 and O2, O4 donor atoms in a distorted ‘pentagonal pyramidal’ geometry (Figure S12).

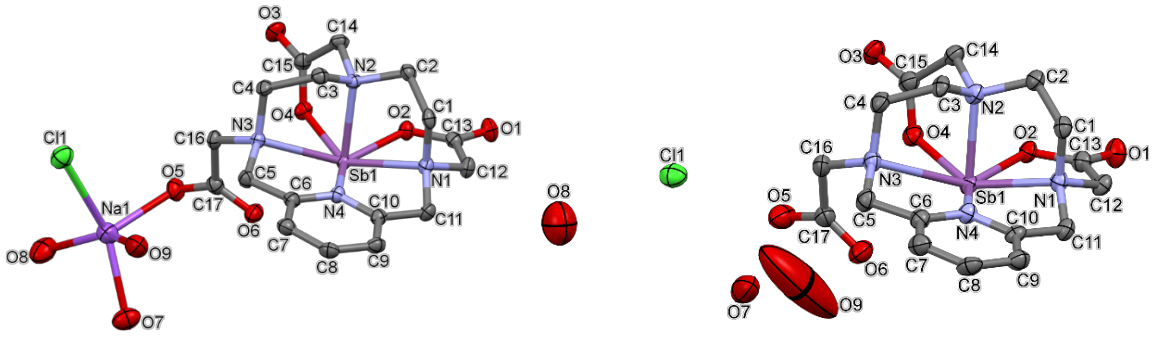

Figure 4. ORTEP representation of the PCTA-Sb1 (left) and PCTA-Sb2 (right) structures with atom labelling. Displacement parameters are shown at 50% probability level. Hydrogen atoms are omitted for clarity

Selected bond lengths and angles of the Sb(III) coordination sphere are collected in Table 1. The water molecules, as well as the chloride in PCTA-Sb1, are coordinated to the Na^+ center, whereas the water molecules are present as the water of crystallization in PCTA-Sb2 located by a well-structured system of intermolecular interactions.

All three carboxylic acid groups in the PCTA-Sb1 complex are deprotonated to maintain the overall neutral charge of the molecule. On the other hand, two of the three carboxylate groups which coordinate to the Sb(III) in PCTA-Sb2 are deprotonated, and the third carboxylate group (C16O5O6) of $PCTA^{3-}$ remains protonated (Figure S13), so H5 could be found on the difference Fourier maps. Comparison of the two crystal structures (Figure S13) explains why sodium ion is captured and embedded in the crystal lattice so easily and why both structures (PCTA-Sb1 and PCTA-Sb2) display very similar unit cell parameters (Table S1). In the opposite side of the filled inner coordination sphere of Sb(III) the chloride anion gets close to the metal center in both structures. If Cl^- also coordinates to the sodium ion as it does in PCTA-Sb1, the Sb…Cl distance is longer. In PCTA-Sb2 the Cl^- has more freedom of motion and is closer to the metal center (Figure S21), but on the basis of Sb….Cl distances (3.420(1) and 3.213(2) Å for the PCTA-Sb1

and PCTA-Sb2, respectively), the coordination to the antimony is unlikely. Since the acetate (O5) pendant arm obviously coordinates to the Na^+ or H^+, the [Sb(PCTA)] complex features a positive charge. This is neutralized by the Cl^- ion in both cases which is probably linked to the whole positively charged complex itself with a weak ionic interaction.[28] Further details on the structures can be found in the Supporting Information (Figure S14-S23) on the unit cells, packing arrangements, coordination geometries, intermolecular interactions.

The geometry of the $[Sb(HPCTA)]^+$ and [Sb(PCTA)] complexes was optimized by considering the relativistic effect due to the presence of a heavy atom, such as antimony. First, the geometries of the protonated complexes were optimized, then three acetate pendant arms were systematically protonated in terminal and internal positions. Optimized structures are shown in the Supporting Information (Figure S24) with the corresponding Cartesian coordinates (Table S4, S5, S6). From these isomers, the protonation of O6 atom is thermodynamically preferred as it is illustrated in Figure S24. This is in good agreement with the results of X-Ray diffraction, where the carboxylate function containing the O6 oxygen atom does not participate in the metal binding. Further DFT calculations indicated that the ligand is capable of binding the antimony in two different coordination environments (N1, N2, N3, N4, O2, O4 *vs.* N1, N2, N3, N4, O2, O4, O6). The optimized geometries, referring to aqueous solution by using the Polarizable Continuum Model (PCM),[29] are presented in Figure S25, while the corresponding Cartesian coordinates are reported in the Table S7 and S8.

The calculated distances of the metal coordination environment are shown in Table 1. The calculations reveal the formation of hexa- or heptacoordinated complexes and the coordination polyhedra are featured by pentagonal pyramid or capped trigonal prism. The difference between the estimated free energies is relatively high, 87.8 kJ/mol, which indicates that the

heptacoordinated complex is most likely predominant in solution. Although the single crystal diffraction studies confirmed the existence of hexacoordinated complex in solid phase, in solution one can assume that third acetate pendant arm coordinates the Sb(III). This can be readily explained by considering the fact that one of the pendant arms coordinates to the Na^+ in solid phase in the case of PCTA-Sb1. As it is shown in Figure S21, the O5 atom does not participate in the metal binding since the carboxylate of the pendant arm is protonated. Such function is capable of forming a H-bond with a surrounding water molecule. The heptadentate coordination mode results in energetically favorable binding sites for Sb(III) with an optimal coordination of three acetate pendant arms than the hexacoordinated complex, where the Sb(III) is accommodated by the oxygen atoms of two carboxylate functions.

For the heptacoordinated complex, the shortest bond distances around the antimony center correspond to the oxygen atoms of the two carboxylate pendant arms (Table 1). This can be readily explained by considering the hard Lewis character of Sb(III). A rather long bond length was calculated between the antimony center and the pyridine-N reflecting only weak coordination. However, the bond length between the antimony and the nitrogen atom of the macrocycle located in the trans position (N2) to the pyridine N is significantly shorter (Table 1). On the basis of this shortened bond length, it is reasonable to assume that the coordinated carboxylate functions promote the binding of the amine N2.

Table 1. Coordination geometry of Sb(III), selected bond lengths (Å) and angles (°) for PCTA-Sb1 and PCTA-Sb2 determined by XSRD and calculated by DFT.

	PCTA-Sb1	**PCTA-Sb2**	**PCTA-Sb (DFT)**
Sb1-N1	2.483(3)	2.407(4)	2.688
Sb1-N2	2.303(3)	2.288(4)	2.404
Sb1-N3	2.608(3)	2.743(5)	2.534
Sb1-N4	2.512(3)	2.537(4)	2.605
Sb1-O2	2.234(3)	2.148(4)	2.287
Sb1-O4	2.182(3)	2.222(4)	2.107
Sb1-O6	2.812(4)	3.044(5)	2.368
N2-Sb1-N1	74.9(1)	76.2(2)	71.2
N2-Sb1-N3	73.3(1)	72.1(1)	74.0
N2-Sb1-N4	86.5(1)	86.0(2)	84.1
N2-Sb1-O2	79.5(1)	80.6(2)	75.9
N2-Sb1-O4	75.6(1)	75.1(2)	75.1
N1-Sb1-N4	64.5(1)	65.4(1)	61.5
N4-Sb1-N3	65.4(1)	64.6(1)	65.8
N1-Sb1-O2	70.9(1)	72.8(1)	67.7
N3-Sb1-O4	74.9(1)	72.3(1)	76.8
O2-Sb1-O4	76.8(1)	78.6(1)	77.5

The electronic absorption spectrum of the antimony complex was calculated through TD-DFT method using the M06 functional.[30] The comparison between the experimental and the calculated spectrum is given in Figure S26. The experimental spectrum is qualitatively reproduced which implies that the optimization of the geometry was reasonably accurate and confirms the suggested

coordination mode in solution. As expected, most of the calculated transitions fall in the UV and near UV regions and associated to the n → π* and π → π* transitions of the pyridine backbone, however a nonbonding lone pair of electrons of Sb(III) also contributes to the absorption (Figure S27).

The results of DFT calculations are in a good agreement with the experimental data in terms of both bond distances and bond angles. However, there is one significant difference between the DFT and SXRD structures. While the O6 atom does not coordinate either in PCTA-Sb1 or in PCTA-Sb2 to the metal centers, it appears to bind the Sb(III) ion based on the DFT calculations (Figure 5, Table 1).

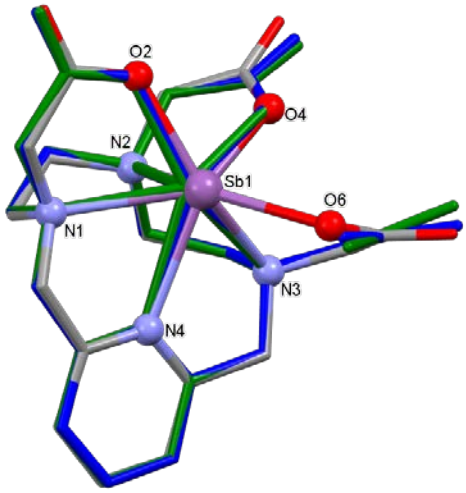

Figure 5. Conformational comparison of PCTA-Sb1 (blue), PCTA-Sb2 (green) and the calculated DFT (colored by elements) structures. The coordination sphere is labelled and highlighted by a ball and stick model. The Na^+ and Cl^- ions, as well as the water molecules are omitted in all structures for clarity.

The estimated bond length between the Sb1-O6 (2.368 Å) is significantly shorter compared to the measured atomic distances of PCTA-Sb1 (2.812(4) Å) or PCTA-Sb2 (3.044(5) Å) which is most probably due to the strong secondary interactions present in the crystal lattices caused by the

sodium ion in case of PCTA-Sb1 and a H-bonded water molecule in case of PCTA-Sb2 (Figure S21). The conformational differences can also be numerically observed in the values of root mean square deviation (RMSD) and maximum atomic distances (Max.D.) of these two compared structures (To compare the agreement between the conformations of the calculated/measured structures, they were overlaid by their same non-hydrogen atoms and characterized by their RMSD and Max.D. values). The comparison of PCTA-Sb1 (blue) and PCTA-Sb2 (green) shows good conformational agreement, as indicated by the RMSD = 0.089 Å and Max.D. = 0.350 Å. Comparing the measured and the calculated structures, for PCTA-Sb1 and the DFT-structure, the RMSD = 0.149 Å, MaxD = 0.404 Å, and for PCTA-Sb2 and the DFT-structure, the RMSD = 0.207 Å and MaxD = 0.570 Å (Figure S23). Noticeably, a pseudo-plane is formed by the contributions of N1, N3, N4, O2 and O4 atoms and the antimony is placed below this plane on the basis of the crystal and DFT calculated structures. The corresponding antimony – pseudo-plane distances are as follows: 0.504 Å for PCTA-Sb1, 0.508 for PCTA-Sb2, 0.564 Å for H1 (ESI) and 0.570 Å for H3 (ESI), respectively. Such formation of pyramid base structures may contribute to the kinetic lability of the [Sb(PCTA)] complex.

Finally, we shortly compare the structure of the [Sb(PCTA)] to the very few structures obtained for aminopolycarboxylate complexes formed with Sb(III). It is obvious that the lone pair electrons have a tremendous effect on the coordination environment of the metal ion.[15] The same distorted pentagonal pyramidal geometry was observed for $EDTA^{4-}$ and $PDTA^{4-}$ complexes of Sb(III)[10,17] and distorted trigonal and tetragonal bipyramidal structures for $HEDTA^{3-}$ [31] and NTA^{3-} [9] chelates respectively, with one coordination site occupied by the unshared electron pair. Furthermore, similar structures were explored for the complexes of O-ligands such as tartrate[32] or oxalate.[33] The

most important aspect of this feature is the inability to cover up the Sb(III) ion completely by donor atoms which could increase the inertness of the Sb(III) complexes against dechelation *in vivo*.

Conclusions

We have demonstrated that the Sb(III) complex of the macrocyclic PCTA ligand possesses thermodynamic stability high enough to prevent the hydrolysis of the Sb(III) near physiological conditions. The equilibrium investigations reveal that the [Sb(PCTA)] complex (being formed under pH=1) goes through two deprotonation steps yielding ternary $[Sb(OH)(PCTA)]^{-}$ and $[Sb(OH)_2(PCTA)]^{2-}$ complexes followed by the hydrolysis of the Sb(III) above pH=9. The formation of the Sb(III) chelate ([Sb(PCTA)] complex) has been confirmed by ESI-MS and NMR measurements while its inertness has been accessed by studying ligand exchange reactions occurring with tartrate as scavenger for the Sb(III). The results of the kinetic study present relatively fast dechelation reactions provoked by OH^{-} ions even in slightly acidic conditions, which is related to the strong tendency of the Sb(III) to hydrolyze and the less compact structure of [Sb(PCTA)] complex (as proved by DFT calculations and X-ray crystallography). X-ray diffraction technique and DFT calculations give further insight into the structural features of the [Sb(PCTA)] complex in solid phase and solution, showing six and seven coordinated Sb(III) complexes, respectively. Thus, [Sb(PCTA)] complex is the first thermodynamically stable antimony(III) complex bearing macrocyclic aminopolycarboxylate platform. In summary, the macrocyclic $PCTA^{3-}$ ligand is not optimal for the complexation of Sb(III), however the thermodynamic and kinetic properties of the complexes based on pyclen platform might be improved by rational ligand design, i.e. by modifying the number, or rather the character of the

donor atoms (e.g. incorporation of S donor atom(s) into the ligands), such efforts are already in progress in our laboratory.

Experimental section

The highest analytical grade chemicals were used for the studies. The Sb(III) stock solution was prepared by dissolving Sb_2O_3 in 6 M HCl resulting a circa 4 M acid content to prevent the formation of hydroxido species. The acid content (and ionic strength) of the stock solution was taken into account in each experiment. The pH of each separate samples was adjusted by NaOH and HCl solutions prepared in the concentration range of 0.2 – 2 M.

The concentration of Sb(III) solution was determined by inductively coupled plasma optical emission spectrometry (ICP-OES 5110 Vertical Dual View, Agilent Technologies). Auto sampler (Agilent SPS4), Meinhard® type nebulizer and double pass spray chamber were used and a five-point calibration procedure was applied (ICP VI, Merck). The ligands were either obtained from commercial sources (H_3NOTA, H_4DOTA, H_5DTPA, H_4CDTA) or prepared by following literature procedures (H_3DO3A, H_2tDO2A, H_2tO2DO2A, H_2BP2A, H_4AAZTA, H_2CDTA-nSer, H_3PCTA).[19,34–39]

Metrohm 888 Titrando titration workstation and a Metrohm-6.0233.100 combined electrode were used to perform the pH-potentiometric titrations. The electrode was calibrated by using KH-phthalate (pH=4.005) and borax (pH=9.177) buffers. The titrated samples (6.0 mL) were kept under inert (N_2) atmosphere to avoid the effect of CO_2. During the titration the solutions were stirred and thermostated (25 °C). The ionic strength of the samples was set to 0.15 or 1.0 M with NaCl. The titrations were carried out by means of 0.2 M NaOH in solutions containing ligand or ligand and metal ion in 1 to 1 ratio (c_L=c_M=2 mM). Because of the high stability of the Sb(III)

complex (the complex formation is complete well below pH = 1.7, the starting pH of the titrated sample) the pH-metric titrations were supported by UV-vis spectrophotometric measurements. For the calculation of the equilibrium constants 100-150 mL–pH data pairs recorded in the pH range of 1.7-12.0 for the ligand and 1.7-8.0 for the complex were used. For the calculation of $[H^+]$ from the pH values, the Irving factor of the electrode was determined by titrating an acid (0.01 M HCl) solution with standardized NaOH.[40] The value of the ion product of water (*K*w) was gained from the same titration (from the pH data collected in the range of 11.2-12.0).

The determination of the stability constant of [Sb(PCTA)] complex was performed by out-of-cell technique. 9 samples were prepared containing the Sb(III) and the PCTA in 0.2 mM concentration, while the $[H^+]$ was in the range of 0.008–1.02 M (I=1.0 M (Na^+ + H^+)). After one day of equilibration, the absorption spectra of the solutions were recorded in the range of 200-400 nm at 25 °C using a Jasco V770 spectrophotometer (Figure S10). The absorbance values measured at 265, 270, 275 and 280 nm were used in the calculation. The equilibrium constants were evaluated by using the PSEQUAD program.[20]

The rate of the decomplexation of [Sb(PCTA)] complex was studied at 25 °C and 0.15 M NaCl ionic strength by following the ligand exchange reactions occurring with tartrate ligand (Jasco V770 spectrophotometer) in the pH range 5.5–7.0 at 275 nm. In order to investigate the effect of the tartrate on the dissociation rate of the Sb(III) complex, the exchange reactions were carried out in the presence of 10-, 20-, and 40-fold excess of that as well ($c_{[Sb(PCTA)]}$=0.2 mM). Furthermore, the high excess of the tartrate ensures the pseudo-first order conditions simplifying the evaluation of the kinetic data. The pH was set by using non-coordinating buffer MES (2-morpholin-4-ylethanesulfonic acid, pK = 6.2) at 50 mM concentration.

For MS measurements maXis II UHR ESI-QTOF MS instrument was used (Bruker, Bremen, Germany) with a CE-ESI Sprayer interface (G1607B, Agilent). Sample introduction was carried out with a 7100 model CE instrument (Agilent, Waldbronn, Germany) using a 70 cm x 75 µm id. capillary (Polymicro, Phoenix, AZ, USA). The MS instrument was controlled by otofControl version 4.1 (build: 3.5, Bruker), spectra were processed by Compass DataAnalysis version 4.4 (build: 200.55.2969, Bruker). MS measurements were performed in positive ionization mode; 0.8 bar nebulizer pressure, 200 °C dry gas temperature, 4.5 L min-1 dry gas flow rate, 3500 V capillary voltage, 500 V end plate offset, 1 Hz spectra rate, 100-1400 m/z mass range were applied. Na-formate calibrant enabled internal m/z calibration.

Following the preparation and lyophilization of the ligand and complex solution, the solid materials were dissolved in deuterium oxide (D_2O), the pD values of the samples were found to be 7.07 and 7.25 for the ligand and complex solution respectively ($c_{PCTA}=c_{[Sb(PCTA)]}=4$ mM). ^1H NMR, diffusion ordered spectroscopy (DOSY) and correlation spectroscopy (COSY) measurements were performed at 298 K by means of a Bruker DRX 400 NMR spectrometer according to the standard pulse programs.[41] Mestrenova software was used to analyse the data.

X-ray diffraction data were collected at 164(2) K on a Rigaku RAXIS-RAPID II diffractometer using Mo-Kα radiation (λ = 0.71075Å). Single crystals were mounted on loops by paratone oil and transferred to the goniometer. Numerical absorption correction[42] was carried out using the program CrystalClear.[43] SHELX program package[44] under Olex2 crystallographic software[45] was used for structure solution and refinement. The structures were solved by direct methods. The models were refined by full-matrix least squares[46] on F^2. It was possible to determine the hydrogen atom positions on the difference Fourier maps. Refinement of non-hydrogen atoms was carried out with

anisotropic displacement parameters. Hydrogen atoms were placed into geometric positions except for the water hydrogens. They were included in structure factor calculations but they were not refined. The isotropic displacement parameters of the hydrogen atoms were approximated from the U(eq) value of the atom they were bonded to. The summary of data collection and refinement parameters are collected in Table S1. All water hydrogens were refined without any further constraints. The water molecules are present as the water of crystallization in PCTA-Sb2 and placed in channels in the PCTA-Sb2 structure which are open in the crystallographic c direction. It explains the high displacement parameters of the water of crystallization molecules and the low crystal quality (Figure S19).

The water molecules are placed in voids of 75.89 $Å^3$ (3.5% of the unit cell) in the PCTA-Sb1, while 358.84 $Å^3$ (16.5% of the unit cell) are available for them in the PCTA-Sb2 complexes. The absence of the Na^+ allows higher freedom of motion of the solvent water molecules in the channels. O9 was also refined in disordered positions, though separation of disordered positions has not resulted a real improvement of the structure as it is a sol heavy atom and the disordered positions are not far from each other. Selected bond lengths and angles of compounds were calculated by PLATON software.[47] The graphical representation and the edition of CIF files were done by Mercury[48] and enCIFer[49] software. Figures for the article were prepared using the Mercury software. Single crystal preparation: 2.5 ml (0.04 M) $PCTA^{3-}$ was dissolved in water and 0.206 ml $SbCl_3$ ($c_{Sb(III)}$=0.485 M, c_{HCl}=4.5 M) was added to the solution. In the case of PCTA-Sb1, the pH of this solution was set to 6 by addition of 0.166 M NaOH solution. For PCTA-Sb2, the pH was not adjusted. The resulting solutions in both cases were evaporated to dryness and absolute methanol was added at room temperature. The white precipitation appeared in the solution was

filtered and the filtrate was taken for the crystallization. Single crystals of [Sb(PCTA)] complexes were grown from methanol solution at room temperature by slow evaporation of the solvent.

The ground state geometry of the complex was computed through Gaussian 09 software package (Rev. C. 01)[50] at DFT level of theory using the hybrid Becke three-parameter B3P86 functional[51] combined with the cc-pwCVTZ-PP basis set for antimony which is based on a small-core pseudopotential,[52] while nitrogen, oxygen and hydrogen atoms were treated by 6-311g(d) basis set. The solvent effect was taken into account by adopting the Polarizable Continuum Model (PCM) for water.[29] Single point calculations were carried out for the ground state geometries which represented true minima on the potential energy surface, thus imaginary frequencies were not found. The electronic transitions were calculated on the geometry optimized for the ground state at TD-DFT level of theory using meta GGA functional, M06, with the same basis set used in the geometry calculation.[30] The predicted electronic spectrum was generated using Gabedit software,[53] while the molecular orbitals (MOs) involved in the transitions were simulated performing Mulliken population analysis (MPA) at the same level of theory used for the optimization.

ASSOCIATED CONTENT

Supporting Information. Details on the thermodynamic and kinetic experiments, NMR and ESI-MS data, details of the X-ray and DFT calculated structures. CCDC 2060909 and 2060910 contain the supplementary crystallographic data for this paper.

AUTHOR INFORMATION

Corresponding Author

*E-mail for Ferenc K. Kálmán: kalman.ferenc@science.unideb.hu

Author Contributions

The manuscript was written through contributions of all authors. All authors have given approval to the final version of the manuscript.

Notes

The authors declare no competing financial interest and there are no conflicts to declare.

ACKNOWLEDGMENT

The research was funded by the Hungarian National Research, Development and Innovation Office (NKFIH K-120224, 128201, 124544, PD-128326 and FK-134551 projects. Eleonóra Dénes thanks Erasmus+ Traineeship for the financial support. N. L. is indebted to the New National Excellence Program of the Ministry for Innovation and Technology from the source of the National Research, Development and Innovation Fund (ÚNKP-20-4-II). The authors are indebted to KIFÜ for awarding access to resource based in Hungary.

REFERENCES

(1) World Health Organization. Cancer. World Health Organization.
(2) Ku, A.; Facca, V. J.; Cai, Z.; Reilly, R. M. Auger Electrons for Cancer Therapy – a Review. *EJNMMI radiopharm. chem.* **2019**, *4* (1), 27.
(3) Peter Bernhardt, Eva Forssell-Arons. Low-Energy Electron Emitters for Targeted Radiotherapy of Small Tumours. *Acta Oncologica* **2001**, *40* (5), 602–608.
(4) Auger, P. V. Sur Les Rayons β Secondaires Produits Dans Un Gaz Par Des Rayons X. *C. R. Acad. Sci.* **1923**, *177*, 169–171.
(5) Bennett, K. T.; Bone, S. E.; Akin, A. C.; Birnbaum, E. R.; Blake, A. V.; Brugh, M.; Daly, S. R.; Engle, J. W.; Fassbender, M. E.; Ferrier, M. G.; Kozimor, S. A.; Lilley, L. M.; Martinez, C. A.; Mocko, V.; Nortier, F. M.; Stein, B. W.; Thiemann, S. L.; Vermeulen, C. Large-Scale Production of ^{119m} Te and ^{119} Sb for Radiopharmaceutical Applications. *ACS Cent. Sci.* **2019**, *5* (3), 494–505.
(6) M. Rey, A. Radiometal Complexes in Molecular Imaging and Therapy. *CMC* **2010**, *17* (31), 3673–3683.

(7) Thisgaard, H.; Jensen, M. Production of the Auger Emitter 119Sb for Targeted Radionuclide Therapy Using a Small PET-Cyclotron. *Applied Radiation and Isotopes* **2009**, *67* (1), 34–38.
(8) Hadjikakou, S. K.; Ozturk, I. I.; Banti, C. N.; Kourkoumelis, N.; Hadjiliadis, N. Recent Advances on Antimony(III/V) Compounds with Potential Activity against Tumor Cells. *Journal of Inorganic Biochemistry* **2015**, *153*, 293–305.
(9) Popov, A. M.; Davidovich, R. L.; Li, I. A.; Skul'beda, A. V.; Hu, S.-Z. Cytotoxic and Antitumor Activity of Antimony(III) Nitrilotriacetate Complexes M2SB(Nta)(HNta) · NH2O (M = NH4, Na; n = 1, 2). *Pharm Chem J* **2005**, *39* (3), 119–121.
(10) Hu, S.-Z.; Tu, L.-D.; Huang, Y.-Q.; Li, Z.-X. Studies on the Antitumor Antimony(III) Aminopolycarboxylic Acid Chelates. Crystal Structures of M[Sb(Pdta)] · H2O (M = Na+, NH4+; Pdta = Propylenediaminetetraacetic Acid). *Inorganica Chimica Acta* **1995**, *232* (1–2), 161–165.
(11) Hsu, B.; Chou, C.; Wang, T.; Liu, M.; Chen, J.; Shen, M. *Kesue Tongbao (Scientia)* **1959**, *22*, 761.
(12) Farina, P.; Levason, W.; Reid, G. Synthesis and Structures of Antimony(III) Halide Complexes with Oxa-Thia and Oxa-Selena Crowns. *Polyhedron* **2013**, *55*, 102–108.
(13) Barton, A. J.; Hill, N. J.; Levason, W.; Reid, G. Synthesis and Structural Studies on Polymeric Assemblies Derived from Antimony(III) Halide Complexes with Bi- and Tri-Dentate and Macrocyclic Thio- and Seleno-Ether Ligands. *J. Chem. Soc., Dalton Trans.* **2001**, No. 10, 1621–1627.
(14) Filella, M.; May, P. M. Critical Appraisal of Available Thermodynamic Data for the Complexation of Antimony(Iii) and Antimony(v) by Low Molecular Mass Organic Ligands. *J. Environ. Monit.* **2005**, *7* (12), 1226.
(15) Ohyama, R.; Takahashi, M.; Takeda, M. Study on Stereochemical Activity of Lone Pair Electrons in Sulfur and Halogen Coordinated Antimony(III) Complexes by 121Sb Mössbauer Spectroscopy. *Hyperfine Interact* **2005**, *161* (1–4), 99–111.
(16) Özer, U. Y.; Bogucki, R. F. Equilibrium Studies of Antimony(III) Chelates in Aqueous Solution. *Journal of Inorganic and Nuclear Chemistry* **1971**, *33* (12), 4143–4153.
(17) Ilyukhin, A. B.; Davidovich, R. L. Effect of a Cation on Stereochemical Activity of Lone Electron Pair in Structures of Ethylenediaminetetraacetatoantimonates(III), Cat[Sb(Edta)]·xH2O[Cat+=Cs,NMe4,1/2(H2En), NH4, Tl, K, 1/2Mn, 1/2Cd, or NH3CH2CH2COOH]. *Kristallografiya* **1999**, *44*, 238–246.
(18) Garda, Z.; Molnár, E.; Kálmán, F. K.; Botár, R.; Nagy, V.; Baranyai, Z.; Brücher, E.; Kovács, Z.; Tóth, I.; Tircsó, G. Effect of the Nature of Donor Atoms on the Thermodynamic, Kinetic and Relaxation Properties of Mn(II) Complexes Formed With Some Trisubstituted 12-Membered Macrocyclic Ligands. *Front. Chem.* **2018**, *6*, 232.
(19) Aime, S.; Botta, M.; Geninatti Crich, S.; Giovenzana, G. B.; Jommi, G.; Pagliarin, R.; Sisti, M. Synthesis and NMR Studies of Three Pyridine-Containing Triaza Macrocyclic Triacetate Ligands and Their Complexes with Lanthanide Ions. *Inorg. Chem.* **1997**, *36* (14), 2992–3000.
(20) Zekany, L.; Nagypal, I. PSEQUAD: A Comprehensive Program for the Evaluation of Potentiometric and/or Spectrophotometric Equilibrium Data Using Analytical Derivatives. In *Computational Methods for the Determination of Formation Constants*; Leggett, D. J., Ed.; Springer US: Boston, MA, 1985; pp 291–353.

(21) Biernat, J.; Ziegler, B.; Zrałko, M.; Kondziela, P. Variability of Some Polarographically Determined Stability Constants. *Journal of Electroanalytical Chemistry and Interfacial Electrochemistry* **1975**, *63* (3), 444–449.
(22) Baes, C. F.; Mesmer, R. E. *The Hydrolysis of Cations*; Wiley: New York, 1976.
(23) Filella, M.; May, P. M. Computer Simulation of the Low-Molecular-Weight Inorganic Species Distribution of Antimony(III) and Antimony(V) in Natural Waters. *Geochimica et Cosmochimica Acta* **2003**, *67* (21), 4013–4031.
(24) Pantani, F.; Desideri, P. G. Il Comportamento Polarografico Dell'antimonio(III) in Soluzione Cloridriche. *Gaz. Chim. Ital.* **1959**, *89*, 1360–1372.
(25) Tian, Q.; Xin, Y.; Yang, L.; Wang, X.; Guo, X. Theoretical Simulation and Experimental Study of Hydrolysis Separation of SbCl3 in Complexation–Precipitation System. *Transactions of Nonferrous Metals Society of China* **2016**, *26* (10), 2746–2753.
(26) Er-kang, W. Polarographic Electrode Process of Antimony(III) Complexes with Complexones. *Collect. Czech. Chem. Commun.* **1982**, *47* (12), 3243–3251.
(27) Kálmán, F. K.; Tircsó, G. Kinetic Inertness of the Mn^{2+} Complexes Formed with AAZTA and Some Open-Chain EDTA Derivatives. *Inorg. Chem.* **2012**, *51* (19), 10065–10067.
(28) Janczak, J.; Kubiak, R. [Phthalocyaninato(2–)]Antimony(III) Chloride. *Acta Crystallogr C Cryst Struct Commun* **2001**, *57* (1), 55–57.
(29) Tomasi, J.; Persico, M. Molecular Interactions in Solution: An Overview of Methods Based on Continuous Distributions of the Solvent. *Chem. Rev.* **1994**, *94* (7), 2027–2094.
(30) Zhao, Y.; Truhlar, D. G. A New Local Density Functional for Main-Group Thermochemistry, Transition Metal Bonding, Thermochemical Kinetics, and Noncovalent Interactions. *The Journal of Chemical Physics* **2006**, *125* (19), 194101.
(31) Li, D.; Zhong, G.-Q. Synthesis and Crystal Structure of the Bioinorganic Complex [Sb(Hedta)]·2H $_2$ O. *Bioinorganic Chemistry and Applications* **2014**, *2014*, 1–7.
(32) Gress, M. E.; Jacobson, R. A. X-Ray and White Radiation Neutron Diffraction Studies of Optically Active Potassium Antimony Tartrate, K2Sb2(d-C4H2O6)2·3H2O (Tarter Emetic). *Inorganica Chimica Acta* **1974**, *8*, 209–217.
(33) Poore, M. C.; Russell, D. R. The Crystal Structure of the [Sb(C2O4)3]3? Ion. A Sterically Active Lone Pair in Six-Co-Ordination. *J. Chem. Soc. D* **1971**, No. 1, 18.
(34) Amorim, M. T. S.; Delgado, R.; da Silva, J. J. R. F. N,N′-Diacetate Derivatives of Some Polyoxa-Polyaza Macrocyclic Compounds: Protonation and Complexation Studies. *Polyhedron* **1992**, *11* (15), 1891–1899.
(35) Kovacs, Z.; Sherry, A. D. A General Synthesis of 1,7-Disubstituted 1,4,7,10-Tetraazacyclododecanes. *J. Chem. Soc., Chem. Commun.* **1995**, No. 2, 185.
(36) Kumar, K.; Chang, C. A.; Francesconi, L. C.; Dischino, D. D.; Malley, M. F.; Gougoutas, J. Z.; Tweedle, M. F. Synthesis, Stability, and Structure of Gadolinium(III) and Yttrium(III) Macrocyclic Poly(Amino Carboxylates). *Inorg. Chem.* **1994**, *33* (16), 3567–3575.
(37) Kim, W. D.; Hrncir, D. C.; Kiefer, G. E.; Sherry, A. D. Synthesis, Crystal Structure, and Potentiometry of Pyridine-Containing Tetraaza Macrocyclic Ligands with Acetate Pendant Arms. *Inorg. Chem.* **1995**, *34* (8), 2225–2232.
(38) Aime, S.; Calabi, L.; Cavallotti, C.; Gianolio, E.; Giovenzana, G. B.; Losi, P.; Maiocchi, A.; Palmisano, G.; Sisti, M. $[Gd\text{-}AAZTA]^-$: A New Structural Entry for an Improved Generation of MRI Contrast Agents. *Inorg. Chem.* **2004**, *43* (24), 7588–7590.
(39) Baranyai, Z.; Garda, Z.; Kalman, F. K.; Krusper, L.; Tircso, G.; Toth, I.; Ghiani, S.; Maiocchi, A. Ethylenediaminetetraacetic Acid Bis(Amide) Derivatives and Their

Respective Complexes with Mn(Ii) Ion for Use as Mri Contrast Agent.: New Substituted Ethylene-Diamine-Tetraacetic-Acid-Bis(Amide) Derivatives and Use Thereof as Ligand Containing Mn (Ii) of Mri Contrast Agent. WO2016135234, 2015.

(40) Irving, H. M.; Miles, M. G.; Pettit, L. D. A Study of Some Problems in Determining the Stoicheiometric Proton Dissociation Constants of Complexes by Potentiometric Titrations Using a Glass Electrode. *Analytica Chimica Acta* **1967**, *38*, 475–488.

(41) Zhou, B.; Shen, M.; Bányai, I.; Shi, X. Structural Characterization of PEGylated Polyethylenimine-Entrapped Gold Nanoparticles: An NMR Study. *Analyst* **2016**, *141* (18), 5390–5397.

(42) NUMABS: Higashi, T. (1998), rev. 2002. (Rigaku/MSC Inc.). .

(43) CrystalClear SM 1.4.0 (Rigaku/MSC Inc., 2008). .

(44) SHELXL: Sheldrick, G.M. (2013) SHELXL-2013 Program for Crystal Structure Solution, University of Göttingen, Germany. .

(45) Dolomanov, O. V.; Bourhis, L. J.; Gildea, R. J.; Howard, J. A. K.; Puschmann, H. *OLEX2* : A Complete Structure Solution, Refinement and Analysis Program. *J Appl Crystallogr* **2009**, *42* (2), 339–341.

(46) Sheldrick, G. M. A Short History of *SHELX*. *Acta Crystallogr A Found Crystallogr* **2008**, *64* (1), 112–122.

(47) Spek, A. L. Single-Crystal Structure Validation with the Program *PLATON*. *J Appl Crystallogr* **2003**, *36* (1), 7–13.

(48) Macrae, C. F.; Edgington, P. R.; McCabe, P.; Pidcock, E.; Shields, G. P.; Taylor, R.; Towler, M.; van de Streek, J. *Mercury* : Visualization and Analysis of Crystal Structures. *J Appl Crystallogr* **2006**, *39* (3), 453–457.

(49) Allen, F. H.; Johnson, O.; Shields, G. P.; Smith, B. R.; Towler, M. CIF Applications. XV. *EnCIFer* : A Program for Viewing, Editing and Visualizing CIFs. *J Appl Crystallogr* **2004**, *37* (2), 335–338.

(50) Frisch, M. J.; Trucks, G. W.; Schlegel, H. B.; Scuseria, G. E.; Robb, M. A.; Cheeseman, J. R.; Scalmani, G.; Barone, V.; Mennucci, B.; Petersson, G. A.; Nakatsuji, H.; Caricato, M.; Li, X.; Hratchian, H. P.; Izmaylov, A. F.; Bloino, J.; Zheng, G.; Sonnenberg, J. L.; Hada, M.; Ehara, M.; Toyota, K.; Fukuda, R.; Hasegawa, J.; Ishida, M.; Nakajima, T.; Honda, Y.; Kitao, O.; Nakai, H.; Vreven, T.; Montgomery Jr., J. A.; Peralta, J. E.; Ogliaro, F.; Bearpark, M. J.; Heyd, J.; Brothers, E. N.; Kudin, K. N.; Staroverov, V. N.; Kobayashi, R.; Normand, J.; Raghavachari, K.; Rendell, A. P.; Burant, J. C.; Iyengar, S. S.; Tomasi, J.; Cossi, M.; Rega, N.; Millam, N. J.; Klene, M.; Knox, J. E.; Cross, J. B.; Bakken, V.; Adamo, C.; Jaramillo, J.; Gomperts, R.; Stratmann, R. E.; Yazyev, O.; Austin, A. J.; Cammi, R.; Pomelli, C.; Ochterski, J. W.; Martin, R. L.; Morokuma, K.; Zakrzewski, V. G.; Voth, G. A.; Salvador, P.; Dannenberg, J. J.; Dapprich, S.; Daniels, A. D.; Farkas, Ö.; Foresman, J. B.; Ortiz, J. V.; Cioslowski, J.; Fox, D. J. Gaussian 09, Gaussian, Inc.: Wallingford, CT, USA, 2009. .

(51) Becke, A. D. Density-functional Thermochemistry. III. The Role of Exact Exchange. *The Journal of Chemical Physics* **1993**, *98* (7), 5648–5652.

(52) Hill, J. G.; Peterson, K. A. Gaussian Basis Sets for Use in Correlated Molecular Calculations. XI. Pseudopotential-Based and All-Electron Relativistic Basis Sets for Alkali Metal (K–Fr) and Alkaline Earth (Ca–Ra) Elements. *The Journal of Chemical Physics* **2017**, *147* (24), 244106.

(53) Allouche, A.-R. Gabedit-A Graphical User Interface for Computational Chemistry Softwares. *J. Comput. Chem.* **2011**, *32* (1), 174–182.

Table of Content

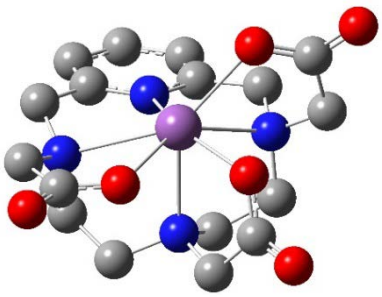

Synopsis:

By pursuing the aim of identifying new antimony(III) complexes, whose ^{119}Sb isotope could be a suitable low-energy electron emitter for radiotherapy, thorough coordination chemical characterization is reported on the first cyclic aminopolycarboxylate complex of antimony(III), [Sb(PCTA)].